

Spatio-temporal quantification of climate model errors in a Bayesian framework

Maeregu Woldeyes Arisido · Carlo Gaetan ·
Davide Zanchettin · Jorge Lopez Parages ·
Angelo Rubino

Received: date / Accepted: date

Abstract Numerical output from coupled atmosphere-ocean general circulation models is a key tool to investigate climate dynamics and the climatic response to external forcings, to predict climate evolution and to generate future climate projections. Coupled climate models are, however, affected by substantial systematic errors or biases compared to observations. Assessment of these systematic errors is vital for evaluating climate models and characterizing the uncertainties in projected future climates. In this paper, we develop a spatio-temporal model based on a Bayesian hierarchical framework that quantifies systematic climate model errors accounting for their underlying spatial coherence and temporal dynamics. The key feature of our approach is that, unlike previous studies that focused on empirical and spatial assessment, it simultaneously determines the spatial and temporal features of model errors and their associated uncertainties. This is achieved by representing the spatio-temporally referenced data using weighting kernels that capture the spatial variability efficiently while reducing the high dimensionality of the data, and allowing the coefficients linking the weighting kernels to temporally evolve according to a random walk. Further, the proposed method characterizes the systematic bias in the mean state as the time-invariant average portion of the spatio-temporal climate model errors. To illustrate our method, we present an analysis based on the case of near-surface air temperature over the tropical Atlantic and bordering region from a multi-model ensemble mean of historical simulations from the fifth phase of the Coupled Model Intercomparison Project. The results demonstrate the improved characterization of climate model errors and identification of non-stationary temporal and spatial patterns.

M.W. Arisido (✉)
University of Milano-Bicocca, via Cadore 48, 20900 Monza, Italy
E-mail: maeregu.arisido@unimib.it
Tel.: +393665067068

C. Gaetan · D. Zanchettin · J. L. Parages · A. Rubino
Department of Environmental Sciences, Informatics and Statistics, Ca' Foscari University of Venice, Via Torino 155, 30172 Venice, Italy

30 **Keywords** Bayesian hierarchical method · Climate model · Climate model errors ·
31 CMIP5 · Spatial statistics · Spatio-temporal model

32 **1 Introduction**

33 Coupled climate models use mathematical approximations of physical and biogeo-
34 chemical processes to simulate the transfer of energy and mass within and across
35 the various compartments of the climate system (Flato et al. 2013). Numerical sim-
36 ulations performed with such models are used to investigate climate dynamics and
37 the climatic response to external forcings, to predict climate evolution and to gener-
38 ate future climate projections, where climate changes as a result of natural as well
39 as anthropogenic forcings can be investigated (Tebaldi et al. 2005; Flato et al. 2013).
40 Despite their continued improvements in representing atmospheric and oceanic phys-
41 ical processes, simulations performed with the current generation of coupled climate
42 models suffer from substantial deficiencies (e.g., Hooten et al. 2008). Among these,
43 of special relevance are the systematic errors that affect the mean state, seasonal-
44 ity and interannual-to-decadal variability simulated by climate models compared to
45 observations (Hawkins et al. 2014; Wang et al. 2014). These systematic errors are
46 commonly referred to as climate model biases (e.g., Cannon 2017).

47 Systematic climate model errors develop due to inadequate representation of rele-
48 vant oceanic and atmospheric processes in climate models (e.g., Hawkins et al. 2014).
49 These imperfections are largely attributed to either the limited understanding of many
50 of the interactions and feedbacks in the climate system or to numerical oversimplifi-
51 cations of well-known processes, so-called parameterizations (Jun et al. 2008). One
52 of the most serious errors shared by climate models is the strong warm sea-surface
53 temperature bias in the south-eastern part of the tropical Atlantic (Flato et al. 2013).
54 Multiple causes have been identified at its origin, in different models, including lo-
55 cal factors, such as the along-shore wind-stress and surface heat fluxes (e.g., Wahl
56 et al. 2015; Milinski et al. 2016), and larger-scale or even remote phenomena, such
57 as the propagation into the south eastern tropical Atlantic of downwelling anomalies
58 generated at the equator (e.g. Toniazzo and Woolnough 2014).

59 Due to the severity of climate model errors, and their unavoidable impacts on
60 the quality of the simulations, error identification, quantification and correction have
61 become relevant topics of applied climate research (Cannon 2017). In general, cur-
62 rent analytic approaches to evaluation and correction of coupled climate model errors
63 determine how much the distributional properties of a climatically relevant quantity
64 obtained from a climate simulation - or analogously from an ensemble of climate sim-
65 ulations - differ from those obtained from observational data for a certain time period
66 and spatial domain (e.g., Jun et al. 2008; Liu et al. 2014). To this purpose, various
67 statistical techniques have been proposed, including the empirical analysis of varying
68 complexity (Richter and Xie 2008; García-Serrano et al. 2012; Grodsky et al. 2012)
69 and bias estimation on a grid point by grid point basis (e.g., Boberg and Christensen
70 2012). Further, research interests on a Bayesian hierarchical assessment of climate
71 model errors are increasing. The Bayesian paradigm allows quantifying systematic
72 errors using full probabilistic inferences based on the posterior distributions derived

from the proposed method. Recent studies focusing on the Bayesian estimation of climate model errors using spatially aggregated geophysical data includes Tebaldi et al. (2005), Buser et al. (2009) and Buser et al. (2010). Furthermore, Arisido et al. (2017) devised a purely spatial Bayesian hierarchical model using gridded data to determine the underlying spatial patterns in climate model biases, thus resolving the limitations of previous works that relied on spatial aggregation or grid-points separately.

In this paper, we develop a spatio-temporal model based on a Bayesian hierarchical approach in order to characterize and quantify climate model errors by explicitly accounting for their spatial and temporal dependencies within a single framework. Spatio-temporal characterization of climate model errors is motivated by the fact that such errors feature the same spatial and temporal complexity of the simulated climate itself, as both, climate and errors, stem and evolve based on the same numerical representation of physical processes. To determine the spatial and temporal features of model errors, and their associated uncertainties, we represent the spatio-temporally referenced data using a set of weighting kernels (e.g., Higdon 1998) that capture the spatial variability efficiently while reducing the high dimensionality of the relatively large-scale data. Our model specification is tailored to the well established state-space approach (Durbin and Koopman 2012), in which the spatio-temporal climate model error process is treated as a time series of non-stationary spatial fields where space is assumed as continuous and time is discrete (Finley *et al.* 2012; Banerjee *et al.* 2014). We characterize the time-invariant systematic bias in the mean state as the average portion of the spatio-temporally varying climate model errors.

To illustrate our method, we present an analysis based on the case of annual-average near-surface air temperature for the period 1948–2005 over the tropical Atlantic and bordering regions from a multi-model ensemble mean of historical simulations from the fifth phase of the Coupled Model Intercomparison Project (CMIP5, Taylor et al. 2012). We use the ensemble mean of the six CMIP5 historical simulations used in Arisido et al. (2017). Focus on the ensemble mean allows reducing the complexity of the Bayesian treatment and attributing the temporal component of the error to the observed internal variability.

In the next section, we describe the data. In Section 3, we present the methodology: definition of climate model errors and our formulation of the Bayesian spatio-temporal method. Section 4 illustrates the results of the analysis. We provide a concluding discussion in Section 5.

2 Data

The dataset comprises observational data and climate model outputs. The latter are obtained from deterministic numerical models, and it is a common practice to consider the model output as data. We use monthly-mean data obtained from the NCEP reanalysis (Kalnay *et al.* 1996) as our observational reference data. Reanalysis data are the output of a state-of-the-art analysis/forecast system with data assimilation using past data from 1948 to the present. The data were provided by the NOAA/OAR/ESRL₁₃ PSD, Boulder, Colorado, USA. Although reanalysis data are not direct observations, they facilitate the purpose of this study, which requires gridded records of absolute

temperatures. Our climate model outputs are originally based on monthly-mean data from an ensemble of six *historical* full-forcing climate simulations contributing to CMIP5. Interested readers are referred to Zanchettin et al. (2015) for a detailed description of the models' characteristics. The data covers the period 1948-2005, for which we derive yearly-mean time series of both observations and simulations over the tropical Atlantic and bordering regions, which is defined geographically as the region covering the latitude range 40°S to 40°N and the longitude range 50°W to 30°E.

3 Methods

3.1 Definitions and notations

Climate model error (hereafter referred to as deviation) is determined by comparing output data simulated from the climate models against observations. We let $Y_t(\mathbf{s})$ and $X_t(\mathbf{s})$ to represent the observed and the simulated value of a certain geophysical quantity, respectively, at spatial location \mathbf{s} , $\mathbf{s} \in \{\mathbf{s}_1, \dots, \mathbf{s}_n\}$ in a region $\mathcal{D} \in R^2$ and time t , $t \in \{1, \dots, T\}$. We derive the spatio-temporal climate model deviation as

$$D_t(\mathbf{s}) = Y_t(\mathbf{s}) - X_t(\mathbf{s}), \quad t = 1 \dots, T \quad (1)$$

where $D_t(\mathbf{s})$ denotes the deviation of the simulated value relative to the observations at spatial location \mathbf{s} and time t . For n spatial locations in \mathcal{D} , we observe the deviations $D_t(\mathbf{s}_1), \dots, D_t(\mathbf{s}_n)$ for the time t . Generally, statistical analysis of climate model deviations can be affected by the spatial misalignment between observations and model output since the model output and the observations are on different grids. We tackle this issue by linearly interpolating the model output data on the regular observational grid to ensure that $Y_t(\mathbf{s})$ and $X_t(\mathbf{s})$ are aligned on the same grid (see, e.g., Gaudard et al. 1999; Jun et al. 2008; Banerjee et al. 2014). One reason for using the linear interpolation method is that both reanalysis and climate model outputs feature high spatial resolution over the investigated domain. We therefore expect that the uncertainty due to the interpolation to minimally affects the results. For each year of the period 1948-2005, we consider a 33×33 ($n = 1089$) grid points. From the spatio-temporal deviation $D_t(\mathbf{s})$, we calculate the empirical *systematic bias* $B(\mathbf{s})$ as $B(\mathbf{s}) = \sum_{t=1}^T D_t(\mathbf{s})/T$. In Figure 1(a), we show this spatially distributed $B(\mathbf{s})$, which is calculated by averaging $D_t(\mathbf{s})$ over the whole period 1948-2005. The spatial pattern of $B(\mathbf{s})$ exhibits the typical features of the climate model bias in the mean state over this study region, including the strong warm bias up to 5 kelvin over the Angola-Benguela front region. Another notable feature is the cold bias over the northern sub-tropics, which is most severe over the Sahara. Figure 1(b) shows the time series, $D(t)$, of the empirical deviation averaged over the considered spatial domain. The time series reflects the evolution of the deviation over the years, in which both short-term and long-term components highlight the portion of observed variability that is not captured by the ensemble-mean evolution. This includes, therefore, observed internal (i.e., spontaneous) variability, which is smoothed out in the ensemble mean. The long-term temporal evolution of $D(t)$ traces that of the Atlantic Multidecadal

Oscillation (AMO), specifically its phase transitions in the 1960s (warm to cold) and 1990s (cold to warm) (e.g. Zanchettin et al. 2016). 156
157

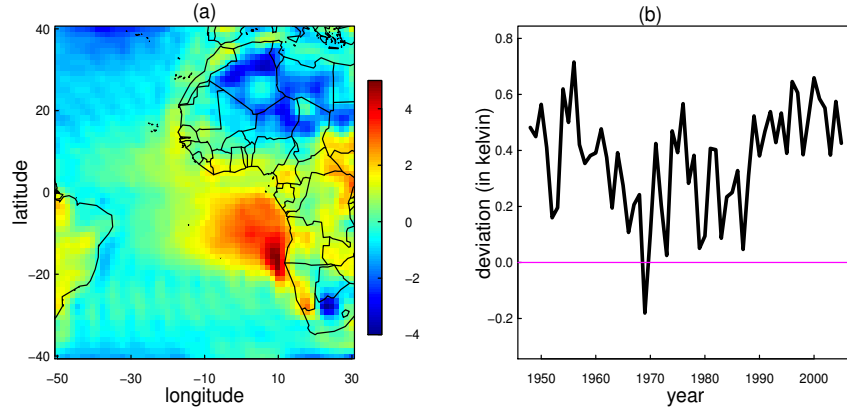


Fig. 1 (a) The systematic empirical bias $B(s)$ in near-surface air temperature over the tropical Atlantic and bordering regions; (b) the temporal deviation $D(t)$, which is obtained by averaging $D_t(s)$ over the spatial domain.

3.2 Bayesian spatio-temporal model for climate model errors

158

The aim here is to formulate a statistical model to quantify and characterize climate model errors accounting for their inherent spatial and temporal dependencies. We specify the model in the Bayesian hierarchical framework based on three levels: *data*, *process*, and *parameters* (see, Berliner 2003; Vanem et al. 2014; Cressie and Wikle 2015, for a comprehensive review). In this setup, our model specification is structured with (1) a data model describing the information given in the form of the empirically observed deviation, conditional on unobserved spatio-temporal deviation process under investigation; (2) the unobserved process featuring spatio-temporal characters described using a set of parameters and (3) the parameters that appear in the first two levels, and specify their prior beliefs according to Bayesian reasoning. 159
160
161
162
163
164
165
166
167
168

169 *3.2.1 Data model*

170 The idea is that in the evaluation of the systematic bias $B(\mathbf{s})$ the local spatio-temporal
 171 effects should be filtered out. To model the deviation, we assume that the observed
 172 deviation $D_t(\mathbf{s})$ can be decomposed into two components:

$$D_t(\mathbf{s}) = M_t(\mathbf{s}) + \varepsilon_t(\mathbf{s}), \quad (2)$$

173 where $M_t(\mathbf{s})$ is a spatio-temporal Gaussian random field and $\varepsilon_t(\mathbf{s})$ is a temporally
 174 and spatially uncorrelated zero mean Gaussian noise with variance σ_t^2 . Note that the
 175 model is allowed to take into account for the heterogeneity in time. We assume that
 176 the noise component $\varepsilon_t(\mathbf{s})$ is independent of the deviation process $M_t(\mathbf{s})$. In practice
 177 we convey into the process $M_t(\mathbf{s})$ all smoothed spatio-temporal components that
 178 actually are blurred by the noise term. We further assume that the observed deviation
 179 $D_t(\mathbf{s})$ is conditionally independent in time given $M_t(\mathbf{s})$. Such assumptions lead to the
 180 data model in the form

$$[D_1(\mathbf{s}), \dots, D_T(\mathbf{s}) | M_1(\mathbf{s}), \dots, M_T(\mathbf{s}), \sigma_1^2, \dots, \sigma_T^2] = \prod_{t=1}^T [D_t(\mathbf{s}) | M_t(\mathbf{s}), \sigma_t^2] \quad (3)$$

181 where $[A]$ denotes the generic notation for the probability distribution of the ran-
 182 dom quantity A . Accordingly $[A|B]$ is the conditional distribution given B .

183 *3.2.2 Process model*

184 The process model characterizes the spatio-temporal deviation process $M_t(\mathbf{s})$. Once
 185 we determine $M_t(\mathbf{s})$, an important interest will be to estimate the more appropriate
 186 time-invariant systematic bias $\tilde{B}(\mathbf{s})$ for the study period as an average of $M_t(\mathbf{s})$, i.e.,
 187 $\tilde{B}(\mathbf{s}) = \sum_{t=1}^T M_t(\mathbf{s})/T$. The spatio-temporal process $M_t(\mathbf{s})$ is driven by a large scale
 188 spatial component that changes stochastically but smoothly in time and a site specific
 189 component. The spatial large scale component at time t is represented by a linear
 190 combination of p spatial kernel functions $\{\psi_k(\mathbf{s}) : k = 1, \dots, p\}$ as in Higdon (1998),
 191 i.e., $\sum_{k=1}^p \psi_k(\mathbf{s}) \beta_{t,k}$, where $\beta_{t,k}$ is the coefficient parameter for kernel k . The whole
 192 formulation is given by

$$M_t(\mathbf{s}) = \psi(\mathbf{s})' \beta_t + v_t(\mathbf{s}) \quad (4)$$

$$\beta_t = \beta_{t-1} + \omega_t \quad (5)$$

$$v_t(\mathbf{s}) = v_{t-1}(\mathbf{s}) + \delta_t(\mathbf{s}) \quad (6)$$

193 where $\psi(\mathbf{s}) = \{\psi_1(\mathbf{s}), \dots, \psi_p(\mathbf{s})\}'$ and $\beta_t = (\beta_{t,1}, \dots, \beta_{t,p})'$. The number of ker-
 194 nels p is chosen to be much less than the number of spatial data points n . The
 195 choice of the kernels is further discussed in section 3.3. Equation (5) states that the
 196 $p \times 1$ vector of the linear coefficients β_t change according to a random walk pro-
 197 cess, where the evolution error ω_t is assumed as an independently and identically
 198 distributed zero mean Gaussian process with variance-covariance matrix Σ_ω . Then,

equation (6) defines the site specific component $v_t(\mathbf{s})$ in order to account for the underlying spatial correlation, capturing its Markovian dependence in time. More specifically, $\delta_t(\mathbf{s})$ follows a zero mean spatial Gaussian process with covariance function C_t , which is specified as $C_t(\mathbf{s}, \mathbf{s}'; \theta_t) = \tau_t^2 \rho(\mathbf{s}, \mathbf{s}'; \phi_t)$, where $\theta_t = \{\tau_t^2, \phi_t\}$ and $\rho(\cdot, \cdot; \phi_t)$ is a correlation function with ϕ controlling the correlation decay and τ_t^2 representing the spatial variance. Any valid spatial correlation function can be used to define $\rho(\cdot, \cdot; \phi)$ (e.g., see Cressie 1993). Here we use the exponential function, i.e., $C_t(\mathbf{s}, \mathbf{s}'; \theta_t) = \tau_t^2 \exp(-\phi_t \|\mathbf{s} - \mathbf{s}'\|)$, where $\|\mathbf{s} - \mathbf{s}'\|$ is the Euclidean distance between locations \mathbf{s} and \mathbf{s}' . Further, for each time point t , ω_t is uncorrelated with $\varepsilon_t(\mathbf{s})$. The different levels of the Bayesian hierarchical approach discussed above can be formulated within a state-space form (Gelfand et al. 2005; Durbin and Koopman 2012). That is, combining the data model (2) and the process models (4)-(6) yields

$$D_t(\mathbf{s}) = \psi(\mathbf{s})' \beta_t + v_t(\mathbf{s}) + \varepsilon_t(\mathbf{s}) \quad (7)$$

$$\beta_t = \beta_{t-1} + \omega_t \quad (8)$$

$$v_t(\mathbf{s}) = v_{t-1}(\mathbf{s}) + \delta_t(\mathbf{s}) \quad (9)$$

where (7) is the measurement equation, and (8,9) are the transition equations. While (7) is similar to the measurement equation of the standard state space model, we recognize that assuming a random walk process in transition equations is a simplification from the more general specification (as provided in, e.g., West and Harrison 1997). Nonetheless the random walk is chosen to provide adequate flexibility for computation and eases the interpretation (e.g., Finley *et al.* 2012).

3.2.3 Parameter model

We complete the model specification by assigning prior probability distributions for the initial conditions $\{\beta_0, v_0(\mathbf{s})\}$ and the model parameters $\{\Sigma_\omega, (\sigma_1^2, \theta_1), \dots, (\sigma_T^2, \theta_T)\}$. Prior distributions for these parameters are generally taken to be non-informative. For the initial conditions, we specify a Gaussian priors in the form $\beta_0 \sim N(\mu_{\beta_0}, \Sigma_{\beta_0})$ where μ_{β_0} is a vector of length p and Σ_{β_0} is a $p \times p$ covariance matrix, and $v_0(\mathbf{s}) = 0$. Recalling $\theta_t = \{\tau_t^2, \phi_t\}$, for the measurement error variance σ_t^2 and the spatial variance τ_t^2 we assign the Inverse-Gamma priors $\sigma_t^2 \sim IG(a_1, b_2)$ and $\tau_t^2 \sim IG(a_2, b_2)$ for each t , where $IG(a, b)$ denotes the inverse gamma distribution with shape parameter a and scale parameter b . Here $\{\mu_{\beta_0}, \Sigma_{\beta_0}, a_1, b_1, a_2, b_2\}$ are called hyperparameters in the Bayesian context, and their values could either be chosen or could be assigned another priors (see, e.g., Gelman 2006). For our analysis, we choose $\mu_{\beta_0} = 0, \Sigma_{\beta_0} = \mathbf{I}_p, a_1 = a_2 = 3$ and $b_1 = b_2 = 100$. For the spatial decay parameter ϕ_t of the exponential spatial correlation function, we assign the uniform prior in the form $\phi_t \sim U(0.001, 0.04)$, which corresponds to the support ranges from 100 to 4000 km. Since the maximum distance between any two locations in the study region is 3030 km, the specified support well covers the full extent of the spatial domain. For the $p \times p$ evolution matrix Σ_ω , we assume the inverse-Wishart prior probability distribution, $\Sigma_\omega \sim IW(p+1, \mathbf{I}_p)$, with the degrees of freedom parameter taking the value $p+1$ and the scale parameter being the $p \times p$ identity matrix \mathbf{I}_p , as we assume

237 independence between the elements of the coefficient vector β_t . These choices corre-
 238 spond to relatively non-informative priors, and our sensitivity analysis indicated that
 239 the results are not substantially sensitive to these choices.

240 3.3 Implementation

241 First we discuss the choice of the spatial kernel vector $\psi(s)$. Several types of kernel
 242 functions have been suggested, including Gaussian kernels (Stroud et al. 2001), har-
 243 monic functions (e.g., Furrer et al. 2007) and bisquare functions (Kang et al. 2012).
 244 In this paper we have considered a Gaussian kernel specified as

$$\psi_k(s) = \exp\{-(s - c_k)' \Sigma^{-1} (s - c_k)/2\}, \quad k = 1, \dots, p \quad (10)$$

245 where c_k denotes the center of the kernel and Σ determines the shape. The num-
 246 ber of kernels p , their locations and shapes must be chosen. These choices are often
 247 based on the presence of prior information such as smoothness and spatial depen-
 248 dence related to the spatial process under study (Stroud et al. 2001). If we choose
 249 spherically shaped kernels, i.e., $\Sigma = \kappa I_2$ on R^2 and $\kappa > 0$, and the centers belong to
 250 a regular grid over an unbounded domain, the resulting spatial process approximates
 251 a covariance function of a stationary isotropic process when the number of kernels
 252 p is very large. Alternatively, a geometrically anisotropic process may be obtained
 253 if we choose non-spherical Gaussian kernels. One way to assess the shape of Σ is
 254 to perform variogram analyses for different directions (see, e.g., Cressie 1993). Our
 255 preliminary analysis using variograms at several time points suggests that isotropy
 256 is a plausible assumption for $M_t(\mathbf{s})$. An example of the variogram plot for $t = 1970$
 257 is shown in Figure 2(a) for the directions: $0^\circ, 45^\circ, 90^\circ, 135^\circ$ (i.e. North, Northeast,
 258 East and Southeast direction, respectively). The variogram does not reveal strong
 259 anisotropy in the four directions at small distances since the patterns are not largely
 260 different from each other. Figure 2(b) shows the $p = 36$ equally-spaced Gaussian
 261 kernels with scale $\Sigma = 0.6I_2$ on R^2 that are used in the main analysis. At the end of
 262 section 4 we further investigate the sensitivity of results for the different choices of
 263 p .

264 Once a reasonable choice of $\psi(s)$ is made, the model can be implemented in the
 265 Bayesian context. For parameter estimation and inference, we seek to obtain the pos-
 266 terior distribution of the unknown parameters $\{\beta_0, \Sigma_\omega, (\beta_1, \sigma_1^2, \theta_1), \dots, (\beta_T, \sigma_T^2, \theta_T)\}$.
 267 For a particular location \mathbf{s} , the posterior distribution can be given in the form

$$\begin{aligned} [\beta_0, \beta_{1:T}, \Sigma_\omega, \sigma_1^2, \theta, \dots, \sigma_T^2, \theta_T | D_{1:T}(\mathbf{s})] \propto \\ \prod_{t=1}^T [D_t(\mathbf{s}) | \beta_t, \sigma_t^2] \times [\beta_0] \times \prod_{t=1}^T [\beta_t | \beta_{t-1}, \Sigma_\omega] \times \\ \prod_{t=1}^T [\sigma_t^2] \times \prod_{t=1}^T [\theta_t] \times [\Sigma_\omega] \end{aligned} \quad (11)$$

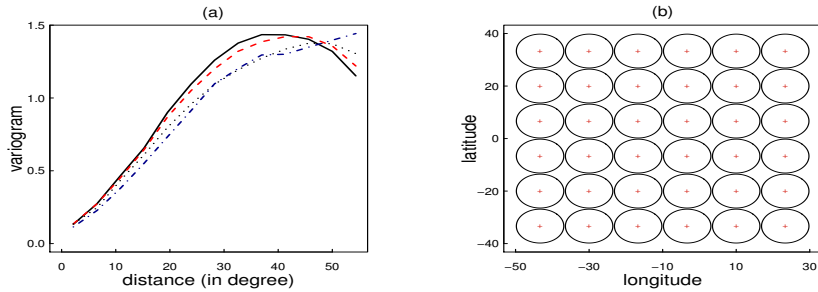


Fig. 2 (a) Empirical variogram for the time $t = 1970$ for the four different directions (black solid 0° , red dashed 45° , gray dotted 90° , blue dashed 135°). The variogram was analyzed using the robust estimator by Cressie (1993); (b) The spherically-shaped 36 equally-spaced Gaussian kernels used for the main analysis. Red crosses indicate the centers of the kernels.

with notations as in Cressie and Wikle (2015). Clearly, the normalizing constant for (11) cannot be found analytically. So, we use the Markov Chain Monte Carlo (MCMC) method (Gilks et al. 1996) with Gibbs sampler and random walk Metropolis steps (Robert and Casella 2013). For the random walk Metropolis step, a multivariate normal (same dimension as the number of model parameters) proposal distribution is used. Based on inspection of graphical tools of the simulation history to assess convergence, we run the Gibbs sampler for 10,000 simulation steps and discarding the first 5,000 as the burn-in period. We performed the analysis using the *spBayes* package (Finley *et al.* 2015) in the freely available R computing environment. The computation time depends mainly on the size of the kernel vectors, the spatial coverage and the number of time points. For example, for our main analysis, a Gaussian kernel vector with length 36, a regular grid of $33 \times 33 = 1089$ sites and $T = 58$ years, the computations take about 40 hours on a 64-bit Unix workstation Intel Xeon 2.60 GHz. We then summarized draws from the posterior MCMC in terms of mean, median and standard deviation to perform posterior inference about the unknowns.

4 Results

Figure 3 shows the posterior means of the spatio-temporal deviation process $M_t(\mathbf{s})$ for the years $t \in \{1950, 1960, 1970, 1980, 1990, 2000\}$. The posterior means are estimated using the 36 Gaussian kernels that are shown in Figure 2(b). These results corroborate the purely spatial results of Arisido et al. (2017) where only the tropical Atlantic was considered. The prominent feature is that the warm error over the southeastern tropical Atlantic persists throughout the simulated period, with maximum value exceeding 4 kelvin over the Angola-Benguela front region and extending westward beyond 10°W . However, the severity of the climate model error estimates is

269
270
271
272
273
274
275
276
277
278
279
280
281
282
283

284
285
286
287
288
289
290
291
292

noticeably different across the years, with differences in the local deviation of more than 1 kelvin (e.g., between 1980 and 1950). The shown exemplary posterior spatial fields reflect an (inter)decadal modulation of the warm error over the south-eastern tropical Atlantic, with alternating decades of strong (roughly 1955-1965, 1980s, and 1995-2005) and moderate (late 1940s-early 1950s, 1970s, early 1990s) errors. Substantial variations through time in the severity of the error are also observed over landmasses, with particularly strong variability over the Sahara.

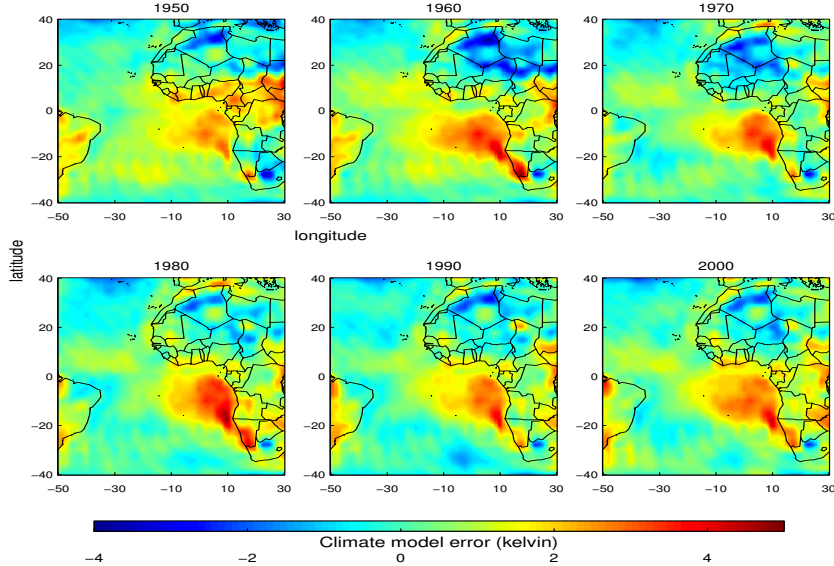


Fig. 3 The posterior means of the spatio-temporal deviation process $M_t(\mathbf{s})$ over the tropical Atlantic and bordering regions for the years $t \in \{1950, 1960, 1970, 1980, 1990, 2000\}$.

The corresponding uncertainty estimates of the posterior $M_t(\mathbf{s})$ are shown in Figure 4, which indicate that the posterior estimates of $M_t(\mathbf{s})$ are most uncertain in the regions affected by cold errors and, more generally, they are more uncertain over land than over the ocean. Particularly, uncertainty is largest in the subsaharan region, with maximum standard error reaching 0.8, which is more pronounced in the period 1960 and 1970, while in 1990 and 2000 the major uncertainties are estimated in the south of the African continent. The posterior estimates of $M_t(\mathbf{s})$ are, conversely, more certain in regions affected by warm errors particularly in the eastern tropical Atlantic ocean, where the minimum standard error is estimated about 0.1. This ocean-land contrast reflects topographic effects and the different spatio-temporal scales of characteristic ocean and land processes.

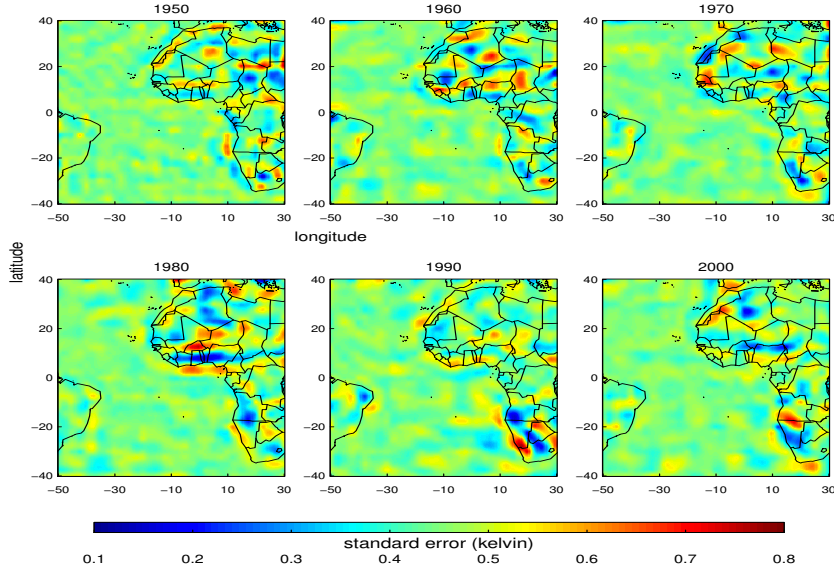


Fig. 4 Posterior standard errors associated to the posterior mean fields of $M_t(\mathbf{s})$, which are shown in Figure 3.

As pointed out in section 3.2.2, the posterior estimate of the systematic bias $\tilde{B}(\mathbf{s})$ is obtained as an average of the posterior $M_t(\mathbf{s})$. Figure 5 presents the posterior $\tilde{B}(\mathbf{s})$ (panel a) and its associated uncertainty estimate (panel b). Overall, the posterior estimate shows warm bias along the Angola-Benguela front region. We notice that the posterior systematic bias $\tilde{B}(\mathbf{s})$ agrees well in its general features, with the empirical bias estimate $B(\mathbf{s})$ (Figure 1a), which implies that our model captures the prominent features in the data. In particular, both $B(\mathbf{s})$ and $\tilde{B}(\mathbf{s})$ capture the warm error over the Angola-Benguela front region and cold error over the western tropical Atlantic ocean, along the South American coast. Nonetheless, the Bayesian spatio-temporal approach allows to gain deeper insights about the climate model error, in particular concerning the spatial dependency of the diagnosed features, and the associated posterior uncertainty estimation. Compared to the empirical estimate, the posterior estimate $\tilde{B}(\mathbf{s})$ displays smoother extended spatial features. The fact that physically consistent features emerge in Figure 5(a), including sharp coastal effects and the signature of oceanic waves, manifests about the detail and quality of the spatial bias estimation allowed by the proposed statistical model. Furthermore, the posterior estimates of uncertainty (5b) highlight regions where quantification of the systematic bias is less certain. Interestingly, despite the overall strong temporal variability diagnosed in the error over the Sahara (Figure 3), uncertainty in the associated systematic bias estimate can be locally relatively small compared to other regions in the studied

311
312
313
314
315
316
317
318
319
320
321
322
323
324
325
326
327
328
329
330

331 domain. In contrast, uncertainty is relatively large for the warm bias over the south-
 332 eastern tropical Atlantic.

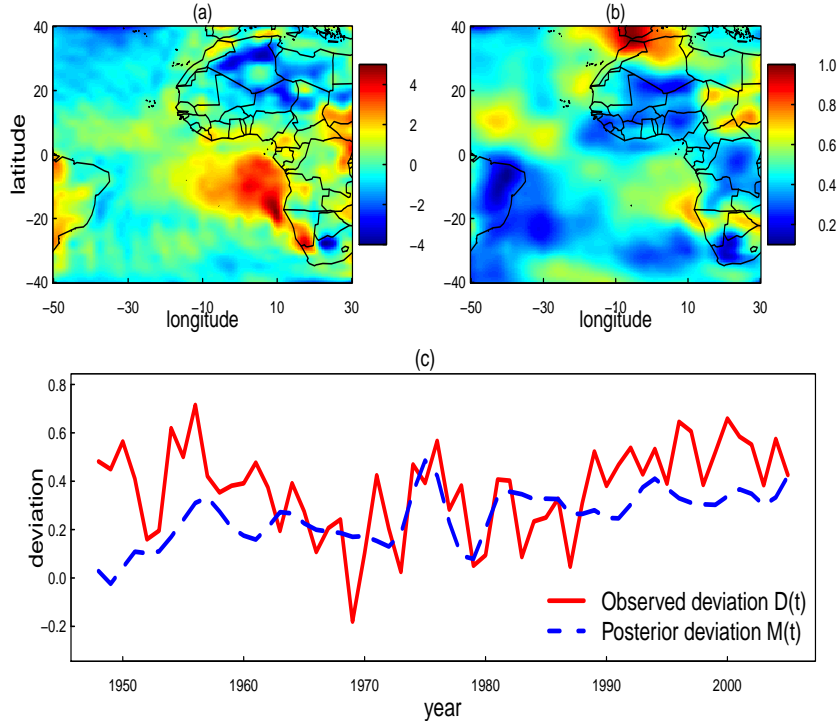


Fig. 5 (a) The posterior systematic bias $\bar{B}(\mathbf{s})$; (b) associated posterior standard error estimate; (c) time series plots of the posterior deviation $M(t)$ obtained as spatially averaged $M_t(\mathbf{s})$, overlay on the corresponding observational deviation $D(t)$ which is also shown in Figure 1(b).

333 To determine the overall temporal character of the spatio-temporal process $M_t(\mathbf{s})$,
 334 Figure 5(c) shows the posterior temporal deviation $M(t)$ as spatially averaged $M_t(\mathbf{s})$
 335 overlay on the corresponding observed deviation $D(t)$. The posterior deviation $M(t)$
 336 appears to be smaller than the corresponding observed deviation $D(t)$. Furthermore,
 337 the posterior estimate has a slowly changing evolution compared with the evolution
 338 of the observed deviation, which in turn suggests the variability in the observed devi-
 339 ation is greater than the variability in the estimate of the posterior deviation.

340 To further assess the posterior estimate of the spatio-temporal process $M_t(\mathbf{s})$ for
 341 more localized features within the study domain, Figure 6 upper panel depicts the
 342 time series trends of the posterior averages of $M_t(\mathbf{s})$ for four subregions, whose lo-
 343 cations are indicated in Figure 6 lower panel. The four subregions are selected for
 344 illustrating the evolution of $M_t(\mathbf{s})$ over: an African land region, the Angola-Benguela
 345 front, an ocean region and a South American land region close to the Atlantic basin.

A trend in a subregion is calculated by averaging the posterior information over the spatial domain of the subregion, where the spatial domain of the subregions are not necessarily equal. The posterior time series of the local deviations indicate that cold bias diagnosed over the landmasses is most severe in the early decades of the analysis, as a long-term warming trend is evident (Trend 2). Over Brazil, where no systematic bias is spotted (Figure 5a), the temporal evolution of the errors indicates a transition from a cold bias to a neutral bias (Trend 1). Similarly, the tropical North Atlantic experiences a sharp transition, around the late 1970s, from a warm bias to a neutral bias situation (Trend 4). As expected, the Angola-Benguela region features the highest warm error over the whole period of study (Trend 3), as for the other locations, featuring a long-term warming trend with superimposed noticeable decadal variability.

346
347
348
349
350
351
352
353
354
355
356
357

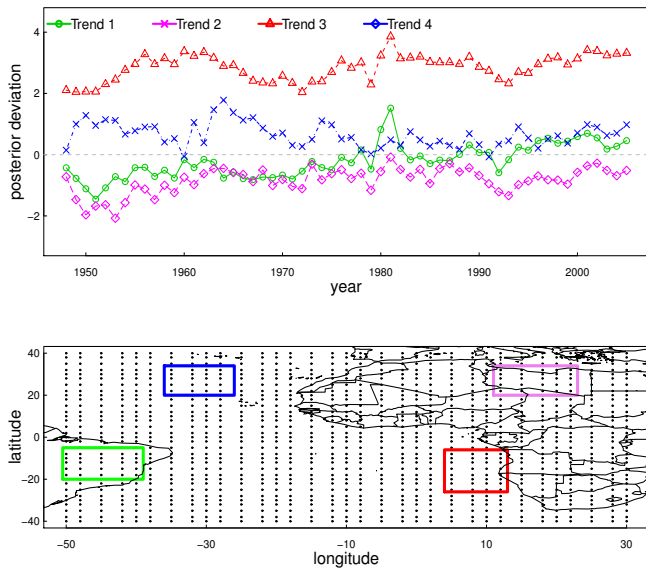


Fig. 6 Time series plots of the posterior average of $M_t(\mathbf{s})$ for selected four different subregions (upper panel) and the locations of the four different subregions (lower panel).

In Figure 7 we show the posterior medians and the associated 95% credible end points for the variance components $\{\sigma_t^2, \tau_t^2\}$. The evolutions of the variance of the observed deviation σ_t^2 (i.e., the nugget in the geostatistical term) and the spatial variance τ_t^2 exhibits temporal variability, supporting our assumption to define time dependent variance parameters to take into account the heterogeneity in time. Additionally, we can see that the spatial variance is greater than the nugget. In fact, the signal-to-noise ratio, which is computed as τ_t^2/σ_t^2 for comparing the strength of the two variance components, is substantially greater than one (not shown), coherent with the hypoth-

358
359
360
361
362
363
364
365

366 esis that the nugget effect is often smaller than the spatial variance (e.g., Bakar and
 367 Sahu 2015).

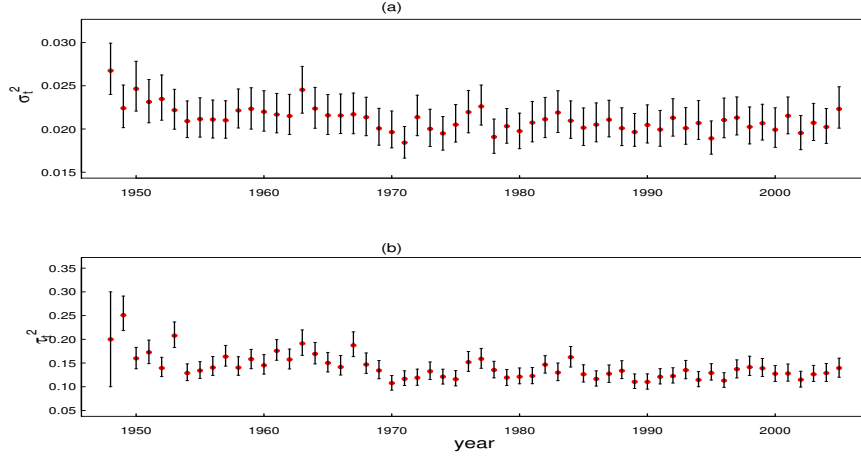


Fig. 7 Posterior median and 95% credible end points for time-varying variance parameters: (a) the variance of the observed data σ_t^2 ; (b) the spatial variance τ_t^2 .

368 Our model specification depends on the use of Gaussian kernel functions to de-
 369 scribe the spatial features of the deviation process $M_t(\mathbf{s})$. We therefore investigate the
 370 adequacy of our model to the choice of Gaussian weighting kernels. The parameters
 371 $\{p, \Sigma, c_k\}$ associated to the kernels may impact the model fit and the prediction. In
 372 particular, the choice of p largely determines the level of spatial detail in the con-
 373 text of dimension reduction techniques (e.g., Finley *et al.* 2012; Arisido *et al.* 2017).
 374 Hence, we perform a sensitivity analysis on the p parameter using three different sets
 375 of kernels, that is $p \in \{16, 30, 48\}$ fixing $\Sigma = 0.5\mathbf{I}_2$, to investigate the sensitivity of
 376 the results to these choices of p . Figure 8 shows the three sets of kernels, along with
 377 the corresponding posterior fields of the deviation process $M_t(\mathbf{s})$. The three different
 378 sets of kernels are shown in column (a). Noticeable differences emerge in the shape of
 379 $M_t(\mathbf{s})$ (column b) including the location and magnitude of the deviation. With $p = 16$,
 380 the larger separation between the kernels results in a strongly smoothed posterior es-
 381 timate. Clearly, the pattern also misses detailed spatial features and misrepresents the
 382 deviation along the Angola-Benguela front, a region known to feature a strong warm
 383 bias. This suggests that a too small number of kernels insufficiently represents the
 384 spatial processes. With larger numbers of kernels, $p = 30$ and $p = 48$, the deviation
 385 process $M_t(\mathbf{s})$ converges to a robust pattern as both choices of p capture well know
 386 features and produce detailed patterns with clearly apparent topographic character-
 387 istics. The fact that both $p = 30$ and $p = 48$ choices lead to very similar posterior
 388 estimates of $M_t(\mathbf{s})$ indicates that the posterior results should not substantially change

if we use $p > 30$. Of course increasing p may allow a better approximation of the deviation process by capturing fine-scale local features. However, the benefit being gained has to be balanced with computational feasibility and the applicability of the model.

389

390

391

392

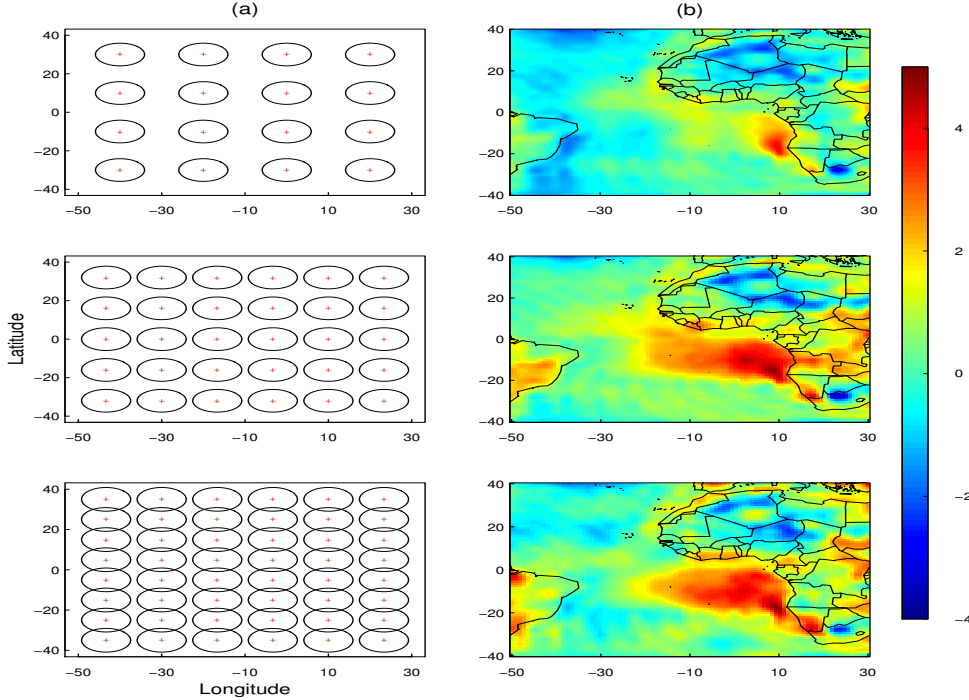


Fig. 8 Comparison of the posterior mean surfaces of the spatio-temporal deviation $M_t(\mathbf{s})$ at year $t = 1985$ for three different choices of the number of kernels p : (a) map of the employed sets of Gaussian weighting kernels; (b) the posterior mean surfaces of $M_t(\mathbf{s})$.

We also analyzed the predictive performance of the model to assess the goodness of the fit. In Figure 9(a) we show a residual, $D_t(\mathbf{s}) - M_t(\mathbf{s})$, surface plot at one randomly selected year. We observe that values of the residual surface plot varies from -0.5 to 0.5 and in most places the fitted values are close to the observations, particularly over the ocean. The largest discrepancies are observed over land, in regions of strong climatic heterogeneity, where the residuals take the form of warm-cold dipoles. Figure 9(b) shows the observation against the posterior median of the time-varying fitted values together with the 95% credible intervals for 10 randomly selected locations. Again we visualize that the fitted values are close to the observations. In fact both the observations and the fitted values lie within the 95% credible bands.

393

394

395

396

397

398

399

400

401

402

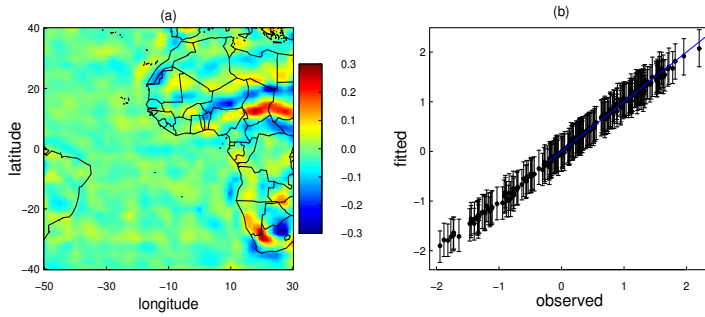


Fig. 9 (a) A residual surface plot at one randomly selected year, (b) observation against the posterior median of the fitted values together with the 95% credible intervals for 10 randomly selected locations.

403 5 Discussion

404 We have proposed a Bayesian spatio-temporal model for assessing errors in coupled
 405 climate models. A key feature of the work presented here is not only quantifying the
 406 errors by accounting for their spatial and temporal dependencies, but also determining
 407 the associated uncertainties using the posterior distributions. Spatio-temporal errors
 408 are characterized as non-stationary spatial fields over a discrete period of time, and the
 409 time-invariant systematic bias in the mean state is estimated as the temporal average
 410 portion of the spatio-temporally varying climate model error.

411 The model was illustrated using the case of near-surface air temperature over
 412 the tropical Atlantic and bordering regions from an ensemble average of six his-
 413 torical simulations contributing to CMIP5. Substantial warm error is estimated over
 414 the southeastern tropical Atlantic with the most severe error found over the Angola-
 415 Benguela front, persisting throughout the simulated period. The posterior analysis
 416 showed that the estimates of the error are more uncertain over landmass than over the
 417 ocean. Particularly, uncertainty is largest in the subsaharan region. Another notable
 418 feature of the results is that the posterior overall temporal evolution in the investi-
 419 gated domain is smaller than the corresponding empirical estimate (see, Figure 5c).
 420 This is due to the fact that our statistical approach quantifies the error process by dis-
 421 entangling the noise component linked to the data and accounting for the underlying
 422 spatial correlation.

The results are consistent with the general consensus of the previous studies of climate model errors (e.g., Wang et al. 2014; Arisido et al. 2017). The generality of the approach presented in this paper suits for the estimation of unknown quantities as well as their prediction for different spatial sites or forecast period. The conditional dependency on the state at the previous time step allows for a straightforward extension of the model to the purpose of error forecasting. In particular, the use of long (spanning several decades) time series allows to obtain precise forecasts with an interannual-to-decadal horizon (West and Harrison 1997).

The proposed statistical model stimulates additional investigation, posing theoretical and computational challenges. For instance, we considered an ensemble average of climate simulations to be representative of climate simulation performances in the study region. A more comprehensive analysis can be envisaged in the form of a multivariate spatio-temporal oriented approach to allow assessments of spatio-temporal simulation errors from several climate models jointly. Furthermore, our approach can be straightforwardly implemented for a broader spatial region and longer time period. However, this bears high computational issue especially as far as the whole globe is considered.

Acknowledgements The research leading to these results has received funding from the European Union, Seventh Framework Programme (FP7/2007-2013) under Grant agreement n 603521 - PREFACE.

Conflict of Interest: The authors declare that they have no conflict of interest.

References

- | | |
|--|--------------------------|
| Arisido MW, Gaetan C, Zanchettin D, Rubino A (2017) A Bayesian hierarchical approach for spatial analysis of climate model bias in multi-model ensembles. Stochastic Environmental Research and Risk Assessment. doi:10.1007/s00477-017-1383-2 | 444
445
446
447 |
| Bakar KS, Sahu SK (2015) sptimer: Spatio-temporal Bayesian modelling using R. Journal of Statistical Software 63:1-32 | 448
449 |
| Banerjee S, Carlin BP, Gelfand AE (2014) Hierarchical modeling and analysis for spatial data. CRC Press, New York | 450
451
452 |
| Berliner LM (2003) Physical-statistical modeling in geophysics. Journal of Geophysical Research (Atmospheres) 108:8776. doi:10.1029/2002JD002865 | 453
454
455 |
| Boberg F, Christensen JH (2012) Overestimation of Mediterranean summer temperature projections due to model deficiencies. Nature Climate Change 2:433-436 | 456
457
458 |
| Buser CM, Knsch HR, Lthi D, Wild M, Schr C (2009) Bayesian multi-model projection of climate: bias assumptions and interannual variability. Climate Dynamics 33:849-868 | 459
460
461 |
| Buser CM, Knsch HR, Weber A (2010) Biases and uncertainty in climate projections. Scandinavian Journal of Statistics 37:179-199 | 462
463 |
| Cannon AJ (2017) Multivariate quantile mapping bias correction: an N-dimensional probability density function transform for climate model simulations of multiple variables. Climate Dynamics. doi:10.1007/s00382-017-3580-6 | |

- 464 Christensen JH, Boberg F, Christensen OB, LucasPicher P (2008) On the need for
465 bias correction of regional climate change projections of temperature and precipi-
466 tation. *Geophysical Research Letters* 35. doi:10.1029/2008GL035694
- 467 Cressie N (1993) Statistics for spatial data. Wiley, New York
- 468 Cressie N, Wikle CK (2015) Statistics for Spatio-temporal Data. John Wiley and
469 Sons, New Jersey
- 470 Durbin J and Koopman, SJ (2012) Time Series Analysis by State Space Methods.
471 Oxford University Press, Oxford
- 472 Finley AO, Banerjee S, Gelfand AE (2012) Bayesian dynamic modeling for large
473 space-time datasets using Gaussian predictive processes. *Journal of Geographical
474 Systems* 14:29-47
- 475 Finley AO, Banerjee S, Gelfand AE (2015) spBayes for large univariate and multi-
476 variate point-referenced spatio-temporal data models. *Journal of Statistical Soft-
477 ware* 63:1-24
- 478 Flato G, Marotzke J, Abiodun B, Braconnot P, Chou SC, Collins W, Cox P, Dri-
479 ouech F, Emori S, Eyring V, Forest C, Gleckler P, Guilyardi E, Jakob C, Kattsov V,
480 Reason C, Rummukainen M (2013) Evaluation of climate models. In: Stocker TF,
481 Qin D, Plattner G-K, Tignor M, Allen SK, Boschung J, Nauels A, Xia Y, Bex V,
482 Midgley PM (eds) Climate change 2013: the physical science basis. Contribution
483 of Working Group I to the Fifth Assessment Report of the Intergovernmental Panel
484 on climate change. Cambridge University Press, Cambridge, United Kingdom and
485 New York, NY, USA
- 486 Furrer R, Sain SR, Nychka D, Meehl GA (2007) Multivariate Bayesian analysis of at-
487 mosphereocean general circulation models. *Environmental and Ecological Statis-
488 tics* 14:249-266
- 489 García-Serrano J, Doblas-Reyes FJ (2012) On the assessment of near-surface global
490 temperature and North Atlantic multi-decadal variability in the ENSEMBLES
491 decadal hindcast. *Climate dynamics* 39:2025-2040
- 492 Gaudard M, Karson M, Linder E, Sinha D (1999) Bayesian spatial prediction. *Envi-
493 ronmental and Ecological Statistics* 6:147-171
- 494 Gelfand AE, Banerjee S, Gamerman D (2005) Spatial process modelling for univari-
495 ate and multivariate dynamic spatial data. *Environmetrics* 16:465-479
- 496 Gelman A (2006) Prior distributions for variance parameters in hierarchical models
497 (comment on article by Brown and Draper). *Bayesian Analysis* 1:515-534
- 498 Gilks WR, Richardson S, Spiegelhalter DJ (1996) Markov chain Monte Carlo in Prac-
499 tice. Chapman and Hall, London
- 500 Grodsky SA, Carton JA, Nigam S, Okumura YM (2012) Tropical Atlantic biases in
501 CCSM4. *Journal of Climate* 25:3684-3701
- 502 Hawkins E, Dong B, Robson J, Sutton R, Smith D (2014) The interpretation and use
503 of biases in decadal climate predictions. *Journal of Climate* 27:2931-2947
- 504 Higdon D (1998) A process-convolution approach to modelling temperatures in the
505 North Atlantic Ocean. *Environmental and Ecological Statistics* 5:173-190
- 506 Hooten MB, Wikle CK (2008) A hierarchical Bayesian non-linear spatio-temporal
507 model for the spread of invasive species with application to the Eurasian Collared-
508 Dove. *Environmental and Ecological Statistics* 15:59-70

- Jun M, Knutti R, Nychka DW (2008) Spatial analysis to quantify numerical model bias and dependence: how many climate models are there?. *Journal of the American Statistical Association* 103:934-947 509
510
511
512
513
514
515
516
517
518
519
520
521
522
523
524
525
526
527
528
529
530
531
532
533
534
535
536
537
538
539
540
541
542
543
544
545
546
547
548
- Kalnay E, Kanamitsu M, Kistler R, Collins W, Deaven D, Gandin L, Iredell M, Saha S, White G, Woollen J, Zhu Y (1996) The NCEP/NCAR 40-year reanalysis project. *Bulletin of the American Meteorological Society* 77:437-471
- Kang EL, Cressie N, Sain SR (2012) Combining outputs from the North American regional climate change assessment program by using a Bayesian hierarchical model. *Journal of the Royal Statistical Society: Series C (Applied Statistics)* 61:291-313
- Liu M, Rajagopalan K, Chung SH, Jiang X, Harrison J, Nergui T, ..., Choate J (2014) What is the importance of climate model bias when projecting the impacts of climate change on land surface processes?. *Biogeosciences* 11:2601-2622
- Milinski SJ, Bader H, Haak AC, Siongco J, Jungclaus H (2016) High atmospheric horizontal resolution eliminates the wind-driven coastal warm bias in the south-eastern tropical Atlantic. *Geophysical Research Letter* 43
- Richter I, Xie SP (2008) On the origin of equatorial Atlantic biases in coupled general circulation models. *Climate Dynamics* 31:587-598
- Robert C, Casella (2013) Monte Carlo Statistical Methods. Springer, New York
- Stroud JR, Mller P, Sansó B (2001) Dynamic Models for Spatiotemporal Data. *Journal of the Royal Statistical Society. Series B, Statistical Methodology* 63:673-689
- Tebaldi C, Smith RL, Nychka D, Mearns LO (2005) Quantifying uncertainty in projections of regional climate change: A Bayesian approach to the analysis of multi-model ensembles. *Journal of Climate* 18:1524-1540
- Toniazzo T, Woolnough S (2014) Development of warm SST errors in the southern tropical Atlantic in CMIP5 decadal hindcasts. *Climate Dynamics* 43:2889-2913
- Vanem E, Huseby AB, Natvig B (2014) Bayesian hierarchical spatio-temporal modelling of trends and future projections in the ocean wave climate with a CO₂ regression component. *Environmental and Ecological Statistics* 21:189-220
- Wahl S, Latif M, Park W, Keenlyside N (2015) On the Tropical Atlantic SST warm bias in the Kiel Climate Model. *Climate Dynamics* 36:891-906
- Wang C, Zhang L, Lee SK, Wu L, Mechoso CR (2014) A global perspective on CMIP5 climate model biases. *Nature Climate Change* 4:201-205
- West M, Harrison PJ (1997) Bayesian Forecasting and Dynamic Models. Springer, New York
- Zanchettin D, Bothe O, Lehner F, Ortega P, Raible CC, Swingedouw D (2015) Reconciling reconstructed and simulated features of the winter Pacific/North American pattern in the early 19th century. *Climate of the Past* 11:939-958
- Zanchettin D, Bothe O, Rubino A, Jungclaus JH (2016) Multi-model ensemble analysis of Pacific and Atlantic SST variability in unperturbed climate simulations. *Climate Dynamics* 47:1073-1090